Bulk Moduli and High Pressure Crystal Structure of U_3Si_2

Xiaofeng Guo[1,2,*], Xujie Lü[2,3], Joshua T. White[4], Chris J. Benmore[5], Andrew T. Nelson[4,6], Robert C. Roback[2], and Hongwu Xu[2,*]

[1] *Department of Chemistry and Alexandra Navrotsky Institute for Experimental Thermodynamics, Washington State University, Pullman, Washington 99164, United States*

[2] *Earth and Environmental Sciences Division, Los Alamos National Laboratory, Los Alamos, New Mexico 87545, United States*

[3] *Center for High Pressure Science & Technology Advanced Research, Shanghai, 201203, China*

[4] *Materials Science and Technology Division, Los Alamos National Laboratory, Los Alamos, New Mexico 87545, United States*

[5] *Advanced Photon Source, Argonne National Laboratory, Argonne, Illinois 60439, United States*

[6] *Fusion and Materials for Nuclear Systems Division, Oak Ridge National Laboratory, Oak Ridge, Tennessee 37830, United States*

---

* Corresponding authors: x.guo@wsu.edu; hxu@lanl.gov

Abstract: U_3Si_2 has been of considerable interest as a high-density light water reactor fuel and is a promising fuel option for generation IV nuclear reactors. Reliable knowledge of the bulk moduli of U_3Si_2 helps understand the mechanical properties, which is needed for predicting the fuel behavior, such as its potential deformation and fracturing, in a reactor operation or accidental circumstance. It also facilitates the modeling efforts by serving as a benchmark parameter. In addition, understanding the high-pressure phase equilibrium is also largely lacking for U_3Si_2. Thus, in this work, we studied the pressure dependence of the crystal structure of U_3Si_2 using high-resolution synchrotron X-ray powder diffraction coupled with Rietveld analysis. The compression of the sample was realized using a diamond anvil cell (DAC) which provides quasi-hydrostatic pressures up to 37.6 GPa. Crystal structural variation and equations of state of U_3Si_2 were obtained, from which its bulk modulus, *a*-axial and *c*-axial moduli were derived to be 107.11 ± 5.65 GPa, 82.87 ± 4.78 GPa and 194.52 ± 12.03 GPa, respectively. The determined elastic anisotropy is compared with that obtained by resonant ultrasound spectroscopy.

Keywords: Uranium silicide; bulk modulus; high pressure; X-ray diffraction; diamond anvil cell

Highlights:

- The high-pressure crystal structure of U_3Si_2 was studied by *in situ* synchrotron X-ray diffraction coupled with the diamond anvil cell technique.
- The bulk modulus, determined by fitting the cell volume data to the Birch-Murnaghan equation of state, was determined to be 107.11 ± 5.65 GPa, and compared to previous experimental and theoretical values.

1. Introduction

Uranium silicides have been considered as alternative fuel materials in Light Water Reactors (LWR), where uranium dioxide (UO_2) is commonly used and in the generation IV nuclear reactors whose safety is improved with enhanced accident tolerance during normal operation or loss-of-coolant events[1-7]. There are many aspects to the advantages of U-Si compounds over UO_2, mainly related to their higher thermal conductivities at operating temperatures and higher uranium densities (*e.g.* 11.05 – 14.7 g U cm^{-3} for U-rich U-Si phases)[2-4, 6, 8]. Among the known U-Si compounds, such as U_3Si, U_3Si_2, USi and U_3Si_5[2-4, 6, 9, 10], U_3Si_2 is of particular interest and has received the major attention due to its relatively high melting point (1938 K)[10], enhanced radiation resistance[11-14], and high thermal stability[7, 15], which are favored for nuclear fuel applications. Disadvantages are that U-Si compounds are generally brittle[5, 16, 17] and susceptible to oxidation[3, 6, 18-20], limiting their full consideration as a preventive solution for nuclear plant disaster scenarios[21], although this can be partially alleviated by the addition of aluminum[18].

U_3Si_2 (space group *P*4/*mbm*) can be treated as a structural derivative of Cu_3Au (space group *Pm*3*m*), where U occupies the Cu site and a pair of Si atoms occupy the Au site[22, 23] (Figure 1a). Density Functional Theory (DFT) calculations by Wang *et al.*[5] show that the bonding features of this intermetallic compound are quite versatile where all three bonding types, ionic, metallic, and covalent bonds, occur via the interactions of U-Si, U-U, and Si-Si, respectively. Such structural characteristics underlie the thermophysical, thermochemical and mechanical properties of U_3Si_2. The temperature-dependent thermal conductivities of U_3Si_2 were studied experimentally up to 1773 K by White *et al.*[3] and theoretically by Zhang *et al.*[24]. The thermal oxidation and phase stability were recently assessed by a number of researchers[3, 6, 18-20, 25]. The enthalpy of formation of U_3Si_2 was previously measured by Alcock and Grieveson[26] and Gross *et al.*[27], and recently re-evaluated to be -33.2 ± 3.1 kJ/mol·at.% by Guo *et al.*[7] using high temperature drop calorimetry.

The elastic properties of U_3Si_2 were measured by Carvajal-Nunez *et al.*[16, 17] but only with a scant dataset, and include the Young's modulus (E = 130.4 ± 0.5 GPa) and the Bulk modulus (K = 68.3 ± 0.5 GPa) from resonant ultrasound spectroscopy (RUS)[16], and E = 153 ± 2 GPa from nanoindentation[17], where the material microhardness was also determined to be 4.5 GPa. However, there is a significant difference between the two reported E values, and the experimentally determined E and K values do not agree well with theoretical calculations[5] where E and K were predicted to be 163.06 GPa and 92.01 GPa, respectively. Therefore, a major objective of this work is to revisit the bulk modulus of U_3Si_2 by performing *in situ* high pressure X-ray diffraction (XRD)[28-36] in which compressibility can be determined intrinsically from pressure-dependent structural variation of U_3Si_2 that is not susceptible to its bulk sample properties, such as porosity, grain characteristics, impurity and sample shape, each of which can affect the elastic properties measured by RUS[16, 37].

The combination of high-energy synchrotron XRD with diamond anvil cell (DAC) techniques allows for the pressure-dependent structural characterization of U_3Si_2 and an evaluation of its phase equilibrium at high pressures. Such studies have been conducted on two other U-Si compounds, USi and USi_2[23], but not on U_3Si_2. In addition, pressure is an important variable to tune the physical properties or even generate emergent functionalities of materials through modifying their crystalline/electronic structures and phase stability relations[38, 39]. Therefore, our high-pressure synchrotron XRD study of U_3Si_2 will lay the foundation for future material optimization studies on the U-Si system via pressure tuning.

2. Experimental Methods

2.1. Sample synthesis and characterization: The starting materials are *1*) U metal containing 31 wppm C impurity with no other impurities detectable by inductively couple mass spectroscopy;

and *2*) silicon powder which is 99.999% pure (Alfa Aesar, USA) without any detectable impurities. U_3Si_2 was synthesized by arc melting of this metallic U and a slight excess of Si (0.1 wt %, to compensate potential Si evaporation at high temperature) in a tri-arc furnace (Centorr Vacuum Industries, Nashua, NH, USA) using methods described previously[3]. The phase purity of our synthesized U_3Si_2 sample was confirmed by ambient XRD (referenced by ICSD No. 31648, Figure 1b) and other characterization techniques[7].

2.2. In situ high pressure, high-energy synchrotron X-ray diffraction experiments and Rietveld analyses: High pressures were generated using a Princeton type symmetric DAC. The sample was loaded in a laser-drilled hole (150 μm diameter) at the center of a pre-indented (40 μm thickness) Inconel gasket, which was encapsulated between two diamonds (culet size 300 μm). Due to the air-sensitivity of U_3Si_2, the loading was conducted in an Ar-flowing glovebox. A gold wire was placed in the sample compartment as the internal pressure calibrant. A 4:1 methanol:ethanol solution (by volume) was used as the pressure transmitting medium. The sample-preloaded DAC was double-contained and then transferred to beamline 6-IDD, at the Advanced Photon Source (APS), Argonne National Laboratory, where the *in situ* high-energy HP-XRD measurements were conducted. The X-ray wavelength was set to 0.123538 Å (100.36 keV), with a beam size of 80 × 80 μm^2. Two-dimensional (2D) diffraction images were collected using an amorphous Silicon area detector (Perkin Elmer XRD 1621), and the geometric parameters calibrated by a CeO_2 standard. The sample to detector distance was fixed at 502.3 mm during experiments. At each pressure point, the sample was exposed to the incident X-rays for 10 s (0.01 s × 1000) to acquire diffraction images with sufficient ring intensities. The obtained 2D diffraction data were corrected for dark current, integrated and calibrated by General Structure Analysis System software version II (GSAS-II)[40] to obtained the patterns that are plotted in intensity as a function of diffraction angle 2θ (Figure 1b). The diffraction patterns were analyzed by the Rietveld method with GSAS-II,

where the instrument parameters were fixed at those obtained fitted by the diffraction peaks of CeO_2, the background by Chebyshev function (10 terms), and the peak profiles to pseudo-Voigt convolution functions.[41] Such procedures were also stated previously elsewhere[38, 42, 43]. The starting structural parameters for refining the structures of U_3Si_2 (ICSD No. 31648), and Au (ICSD No. 52249) under compressing were referred to Zachariasen[44] and Ichikawa[45], and Wyckoff[46], respectively. The final two-phase refinements at each pressure points are convergent. Representative fitted patterns are shown in Figure 2. Two-phase (U_3Si_2 and Au) Rietveld refinements were performed to determine the crystal structures of both phases under high pressures with R_{wp} ranging from 2.9% to 5.5% (Table 1). Their unit-cell parameters and volumes are shown in Table 1. The fitting of equation of state (EOS) based on the structure-pressure experimental data were performed in the EosFit7 program[47, 48].

3. Results and Discussion

Due to some relatively large grains (~100 μm) of the U_3Si_2 sample loaded in DAC, the diffraction images obtained during compression consist of a few sets of single-crystal diffraction spots, which cannot be analyzed as powder XRD data with GSAS-II. However, these large grains were crushed at higher pressures into smaller grains with homogenous distributions in size and orientation, resulting in smooth diffraction rings (Figure 1c) suitable for Rietveld analysis. Thus, we used the XRD data collected during subsequent decompression to derive structural parameters of U_3Si_2 at various pressures.

Pressures were determined from the derived cell volumes of Au based on its equation of state (EOS)[49] (Figure 3a). The uncertainties of the determined pressures are due to the propagation of errors associated with Au cell volumes. With increasing pressure, the unit cell of U_3Si_2 contracts continuously (Table 1), as reflected by the decreases in lattice parameters *a* and *c* (Figure 4).

Moreover, there is no emergence or disappearance of diffraction peaks while increasing pressure to ~40 GPa, suggesting that U_3Si_2 undergoes no noticeable phase transitions. The elastic prosperities of U_3Si_2 can be determined by analyzing the pressure-dependent structural data, especially lattice parameters. The unit cell volume–pressure relation can be fitted by the second order Birch-Murnaghan equation of state[50]:

$$P = \frac{3K_0}{2}\left[\left(\frac{V_0}{V}\right)^{\frac{7}{3}} - \left(\frac{V_0}{V}\right)^{\frac{5}{3}}\right]\{1 + \frac{3}{4}(K_0' - 4)[\left(\frac{V_0}{V}\right)^{\frac{2}{3}} - 1]\}, \quad (1)$$

where V_0 is the zero-pressure cell volume (211.45 ± 1.24 Å^3), slightly (0.9 %) larger than the literature value[45] 209.59 Å^3, V is the cell volume at a given pressure P, and K_0' is the pressure derivative of the isothermal bulk modulus, which is fixed at 4[50]. The bulk modulus (K_0) obtained by a least-squares fit of equation (1) to the experimental P-V data is 107.11 ± 5.65 GPa. This value is much larger than that determined by RUS (68.3 GPa)[16], but is in general agreement with the DFT-derived value, 92.01 GPa[5]. The smaller value from RUS could be a result of sample-dependent bulk characteristics, where weight, impurity, porosity, and symmetrical shape can all contribute to the underestimation[16, 37]. However, even though the method for obtaining K_0 in this work is immune to deviations caused by sample preparation or bulk defects, its accuracy still depends on the confidence of the determined pressures, the (quasi-)hydrostaticity during compression, and the quality of Rietveld refinements that determine the crystal structures.

One way to check the quality of the fitted EOS is comparing its derived bulk modulus with that obtained by linear moduli through the relation[48] $K_{0,lm} = 3 \cdot \left(\frac{1}{M_{a,0}} + \frac{1}{M_{a,0}} + \frac{1}{M_{c,0}}\right)^{-1}$, where $M_{a,0}$ and $M_{c,0}$ are the linear moduli along the a- and c-axis, respectively, which indicate the linear compressibility at zero pressure. Similar to the volume–pressure relation, the variances of unit cell parameters at various pressures can be fitted by the one-dimensional analog of the Birch-Murnaghan equation of state[29] (Figure 4), which is replacing V in equation (1) with a^3 or c^3:

$$P = \frac{3M_{a,0}}{2}\left[\left(\frac{a_0}{a}\right)^7 - \left(\frac{a_0}{a}\right)^5\right],$$

$$P = \frac{3M_{c,0}}{2}\left[\left(\frac{c_0}{c}\right)^7 - \left(\frac{c_0}{c}\right)^5\right], \quad (2)$$

where a_0 and c_0 are parameters at the ambient pressure. The linear moduli can then be derived from the fitted curves of *a* and *c* as a function of pressure to be $M_{a,0}$ = 82.87 ± 4.78 GPa and $M_{c,0}$ = 194.52 ± 12.03 GPa. $K_{0,lm}$ obtained from linear moduli is 102.48 GPa, in general good agreement with K_0, 107.11 GPa. Noted that the linear modulus along *c*-axis is ~ 2.4 times of that along *a*-axis, suggesting that the lattice is less compressible along the *c*-axis. Such anisotropic compressibility is obviously seen in Figure 4 that the rate of contraction in *c* constant is smaller than that in *a* constant, with a decelerating trend at higher pressures.

The anisotropic behavior in axial compressibility can be explained by the susceptibility of bond distance to compression (Figure 5). The atomic coordinates and atomic displacement parameters obtained from the Rietveld analyses are listed in Table 2, from which the evolution of bond lengths under high pressures can be obtained. At the lowest measured pressure, 2.2 GPa, the structure of U_3Si_2 is close to that under the ambient condition (1 atm). There are two types of U atoms situating within two layers parallel to (001) in a unit cell (Figure 1a). In one layer, each U1 atom is coordinated with four in-plane Si atoms as the nearest neighbors (U1-Si = 2.906(6) Å), and the bond distance between the two Si atoms of a covalent Si-Si pair (Si-Si) is 2.51(3) Å. In the other (001) layer, each U2 is surrounded by five other in-plane U2 atoms (U2-U2 = 3.791(6) Å), and bonded to six Si atoms (two Si1 and four Si2 atoms) from neighboring (001) layers with a bond distance of U2-Si = 2.815(9) Å or 2.977(5) Å. These structural parameters are in accordance with experimental[44] and theoretical[5] values. With increasing pressure, in-plane bonds that is perpendicular to *c*-axis behave differently from those out-plane parallel to *c*-axis. As seen from Figure 5, all three in-plane bonds U1-Si, Si-Si, and U2-U2 have large-percentage changes upon

compression that compared to their values under 2 GPa, they contract 6 % ~ 11 % at 30 GPa. On the other hand, the bond interactions along the *c*-axis are more resistant to compression which were evaluated based on the projection of diagonal bonding interactions (U2 and other atoms) that the interatomic distances contract only between 4 % ~ 7 % when pressure increases from 2 GPa to 30 GPa. Thus, the anisotropic axial behavior of bonding among atoms resonates with those seen in the lattice parameters.

Furthermore, we investigated other elastic properties. The shear modulus *G* characterizes the resistance of materials to plastic deformation, which cannot be derived directly by this work. Thus, we used DFT-calculated value $G = 67.68$ GPa[5] in the following derivation. The ratio of K/G defines whether material behavior is ductile or brittle, in which the critical value is around 1.75 for separating these two with higher ratio suggesting ductility[51]. The zero-pressure K_0/G of U_3Si_2 was determined to be 1.58, consistent with 1.36 predicted by DFT calculation[5] and larger than 1.24 derived from RUS measurements[16]. Thus, U_3Si_2 at ambient condition is brittle by the above definition, consistent with the experimental observation[52] and the theoretical prediction[5]. Lastly, the Young's Modulus *E* and Poisson's ratio σ at ambient condition were obtained by the following equation (2) and (3) to be 167.72 GPa and 0.24, respectively:

$$E = \frac{9GK_0}{G+3K_0} \tag{3}$$

$$\sigma = \frac{3K_0-2G}{2(G+3K_0)} \tag{4}$$

E from this work is in excellent agreement with that calculated from DFT, 163.06 GPa[5], which is closer to 153 GPa (nanoindentation)[17], but larger than 130.4 GPa (RUS)[16] by ~27 %. Poisson's ratio σ, describing the extent of contraction over expansion, can be used to index the bonding features with ~0.1 for covalent bonds and ~0.25 for ionic bonds[53, 54]. Therefore, both DAC and DFT work suggest that U_3Si_2 is dominated by the ionic contribution resulting from three different

U-Si bonds, while the conclusion from RUS implies the multiple contributions from ionic and covalent interactions. The comparison of elastic constants derived from this work, RUS and nanoindentation are summarized in Table 3.

4. Conclusions

In this work, we performed the first static compression experiments on U_3Si_2 up to 37.6 GPa and obtained the pressure-dependent crystal structures from *in situ* high pressure, high-energy angle-dispersive X-ray diffraction. The bulk modulus of U_3Si_2 was intrinsically obtained by fitting the Birch-Murnaghan equation of state to the experimentally obtained *P*-*V* relations, to be 107.11 ± 5.65 GPa, which can be used as a benchmark value for future theoretical calculations. Other elastic properties were also evaluated, which were found to be consistent with DFT predictions and nanoindentation data, but agree poorly with RUS-derived values. Future RUS work on high-purity and high-density U_3Si_2 may be needed to validate data obtained from this work.

Acknowledgements

Research presented in this article was supported by the Laboratory Directed Research and Development (LDRD) program of Los Alamos National Laboratory (LANL) under project number 20180007 DR. X.G. acknowledges the support through a LANL Seaborg postdoctoral fellowship and, later, the institutional funds from the Department of Chemistry at Washington State University. LANL, an affirmative action/equal opportunity employer, is managed by Triad National Security, LLC, for the National Nuclear Security Administration of the U.S. Department of Energy under contract 89233218CNA000001. This research used resources of the Advanced Photon Source, a U.S. Department of Energy (DOE) Office of Science User Facility operated for the DOE Office of Science by Argonne National Laboratory under Contract No. DE-AC02-06CH11357.

Tables

Table 1 Unit-cell parameters and refinement agreement indices of U_3Si_2 at high pressures.

	U_3Si_2			Au		
Pressure (GPa)	a (Å)	c (Å)	V (Å^3)	a (Å)	V (Å^3)	R_{wp} (%)
2.2 ± 1.1	7.311(2)	3.883(1)	207.55(9)	4.062(1)	67.00(6)	3.20
3.6 ± 1.1	7.263(3)	3.856(2)	203.41(23)	4.054(1)	66.64(6)	3.18
5.8 ± 1.3	7.231(3)	3.843(2)	200.93(26)	4.042(1)	66.06(7)	2.96
8.1 ± 1.3	7.193(4)	3.829(2)	198.14(26)	4.029(1)	65.40(7)	2.91
10.2 ± 1.3	7.157(4)	3.815(2)	195.40(28)	4.016(2)	64.77(7)	3.05
14.2 ± 1.8	7.088(5)	3.795(3)	190.62(37)	3.992(2)	63.62(10)	3.46
16.9 ± 1.3	7.041(4)	3.778(3)	187.34(26)	3.977(1)	62.89(7)	3.00
19.4 ± 1.5	6.998(4)	3.764(3)	184.32(29)	3.963(2)	62.24(8)	2.90
21.4 ± 1.6	6.967(4)	3.755(3)	182.27(30)	3.953(2)	61.77(9)	2.96
26.9 ± 1.0	6.883(4)	3.737(3)	177.05(21)	3.927(1)	60.55(6)	4.53
30.6 ± 1.0	6.847(3)	3.730(2)	174.91(13)	3.910(2)	59.78(5)	4.80
37.6 ± 1.5	6.735(4)	3.714(3)	168.46(19)	3.881(2)	58.46(8)	5.45

Table 2 Atomic coordinates and atomic displacement parameters of U_3Si_2 as a function of pressure.

	U1(x, y, 0.5)		Si(x, y, 0.0)				
Pressure (GPa)	x	y	x	y	U_{iso}(U1) (Å^2/100)	U_{iso}(U2) (Å^2/100)	U_{iso}(Si) (Å^2/100)
2.2 ± 1.1	0.1803(5)	0.6803(5)	0.6249(26)	0.1249(26)	0.1(2)	3.5(3)	3.8(6)
3.6 ± 1.1	0.1802(6)	0.6802(6)	0.6191(29)	0.1191(29)	0.0(2)	6.2(5)	3.8(6)
5.8 ± 1.3	0.1805(5)	0.6805(5)	0.6198(26)	0.1198(26)	0.2(1)	9.0(6)	4.5(7)
8.1 ± 1.3	0.1786(7)	0.6786(7)	0.6253(11)	0.1156(27)	0.2(1)	9.8(5)	2.6(11)
10.2 ± 1.3	0.1800(6)	0.6800(6)	0.6195(25)	0.1195(25)	0.0(1)	8.9(5)	1.8(6)
14.2 ± 1.8	0.1806(10)	0.6806(10)	0.6166(36)	0.1166(36)	0.3(1)	8.9(11)	2.2(14)
16.9 ± 1.3	0.1770(6)	0.6770(6)	0.6279(29)	0.1279(29)	0.1(1)	8.1(6)	2.6(7)
19.4 ± 1.5	0.1775(5)	0.6775(5)	0.6287(26)	0.1287(26)	0.1(1)	8.1(5)	2.6(7)
21.4 ± 1.6	0.1774(5)	0.6774(5)	0.6291(26)	0.1291(26)	0.1(1)	8.1(6)	2.6(8)
26.9 ± 1.0	0.1741(10)	0.6741(10)	0.6282(56)	0.1286(56)	0.9(1)	8.5(15)	2.6(14)
30.6 ± 1.0	0.1712(11)	0.6712(11)	0.6319(53)	0.1312(53)	1.5(2)	9.4(11)	7.0(22)

Table 3 The bulk modulus values determined from DAC, with comparisons from those calculated from DFT, and derived from RUS and Nano-indentation.

	DFT[5]	RUS[16]	Nano-indentation[17]	DAC (this work)
K (GPa)	92.01	68.3 ± 0.3		107.11 ± 5.65
G (GPa)	67.68	55.2 ± 0.5		
E (GPa)	163.06	130.4 ± 0.5	153.0 ± 2.5	*167.72*[a]
K/*G*	1.36	1.24		*1.58*[a]
σ	0.20	0.182		*0.24*[a]

[a] values are derived based on G = 67.68 GPa taken from DFT work[5].

Figures

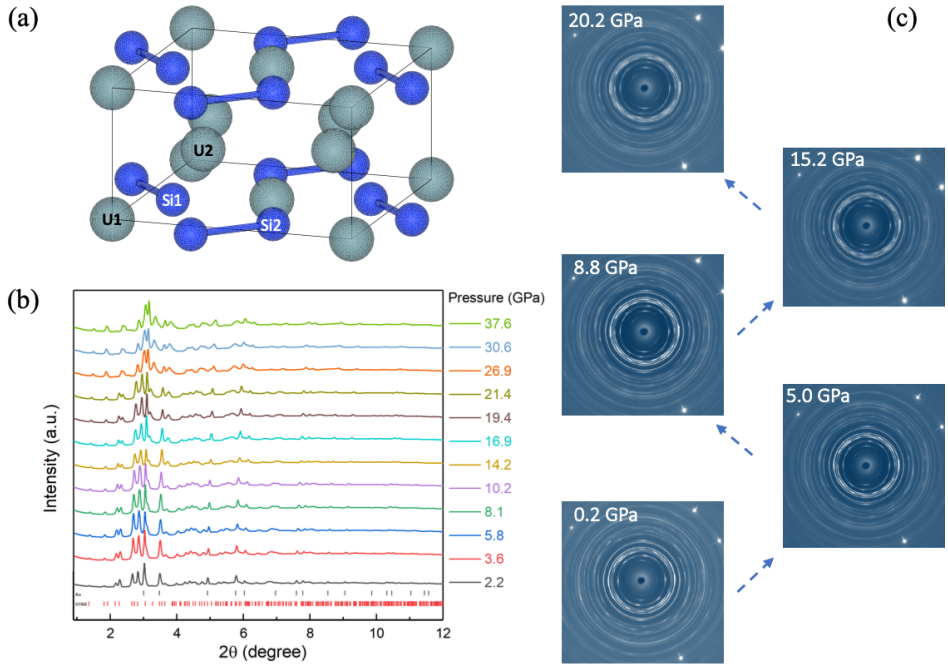

Figure 1. *in situ* structural characterization of U_3Si_2 under high pressures: (a) the crystal structure derived from the ambient diffraction pattern; (b) the integrated 1D diffraction patterns overlapped as a function of pressure up to 37.6 GPa during the decompression; (c) 2D diffraction images at five selected pressure points.

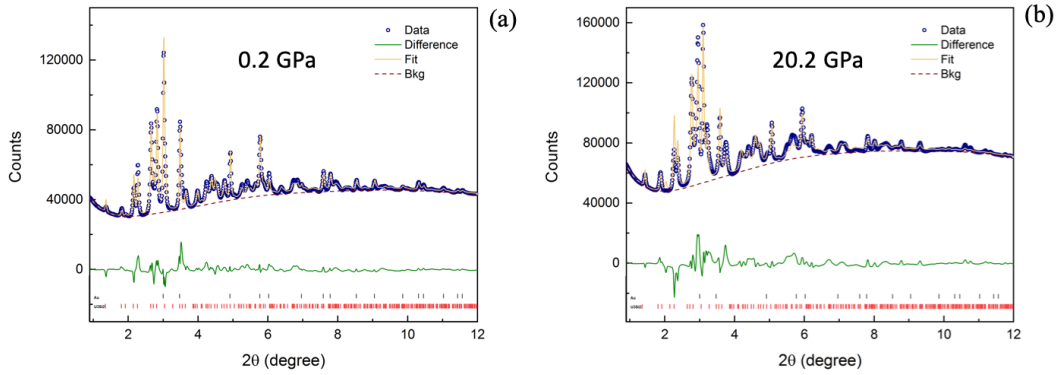

Figure 2. Representative fitted patterns of Au and U_3Si_2 at low and high pressures.

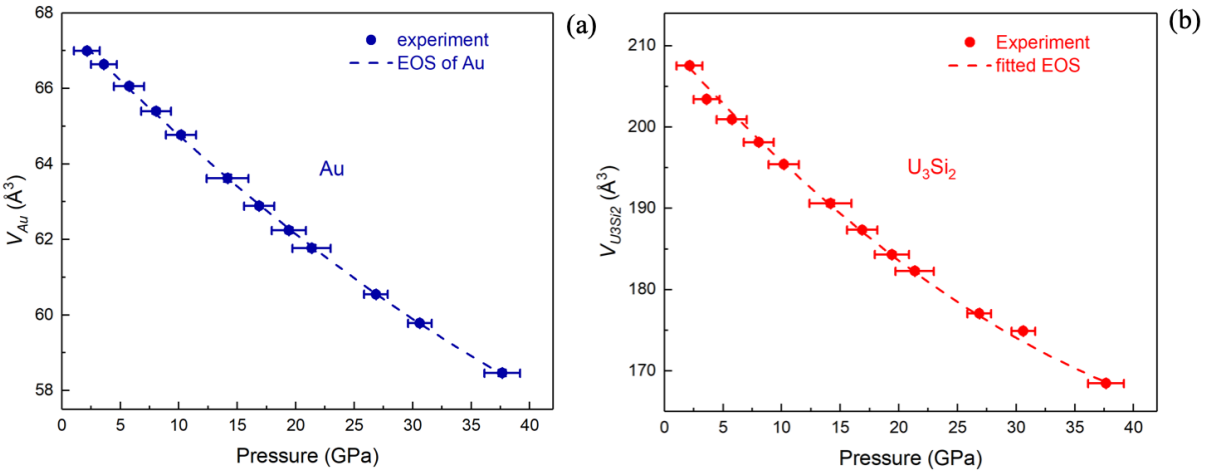

Figure 3. *P-V* relations of Au and U_3Si_2 using the fitted unit cell volumes from the Rietveld refinements: (a) the pressure determined from the equation of state of Au; (b) the fitted equation of state of U_3Si_2 using the Birch-Murnaghan equation.

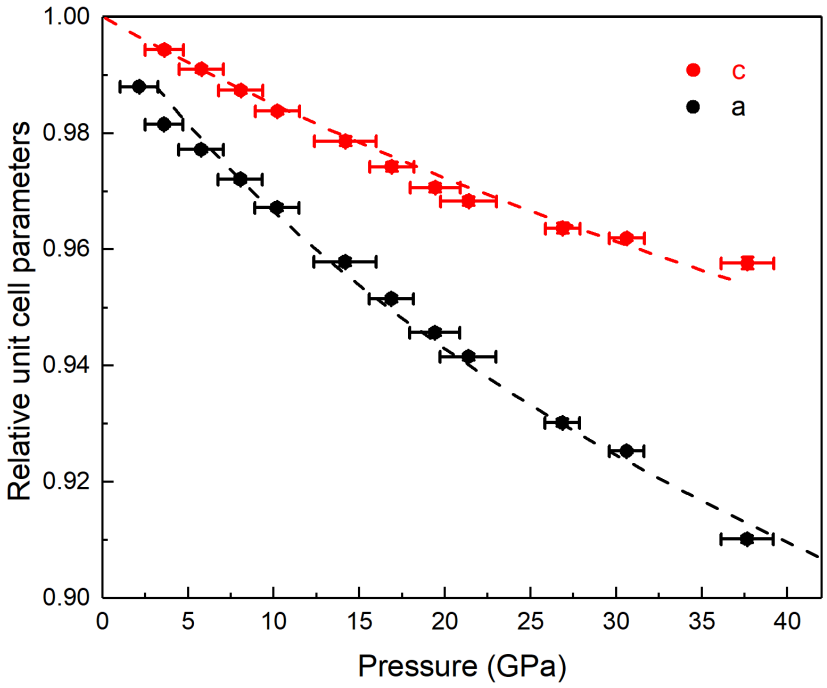

Figure 4. The relative unit cell parameters as a function of pressure.

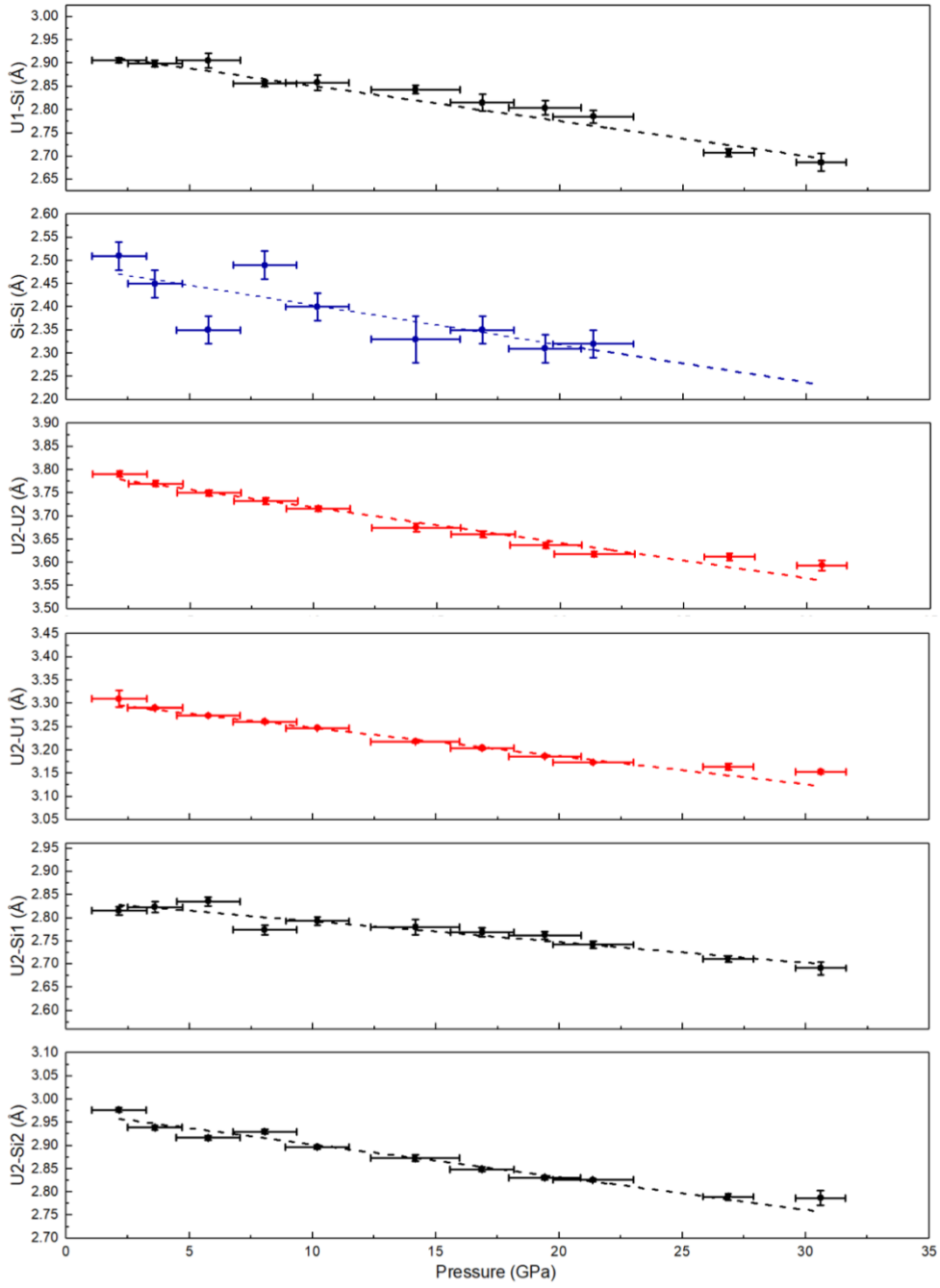

Figure 5. The bonding distance variance as a function of pressure.

References

1. A. Nelson, J. White, D. Byler, J. Dunwoody, J. Valdez and K. McClellan, *Trans. Am. Nucl. Soc.*, 2014, **110**, 987-989.
2. J. T. White, A. T. Nelson, D. D. Byler, D. J. Safarik, J. T. Dunwoody and K. J. McClellan, *J. Nucl. Mater.*, 2015, **456**, 442-448.
3. J. T. White, A. T. Nelson, J. T. Dunwoody, D. D. Byler, D. J. Safarik and K. J. McClellan, *J. Nucl. Mater.*, 2015, **464**, 275-280.
4. J. T. White, A. T. Nelson, J. T. Dunwoody, D. D. Byler and K. J. McClellan, *J. Nucl. Mater.*, 2016, **471**, 129-135.
5. T. Wang, N. Qiu, X. Wen, Y. Tian, J. He, K. Luo, X. Zha, Y. Zhou, Q. Huang and J. Lang, *J. Nucl. Mater.*, 2016, **469**, 194-199.
6. E. S. Wood, J. T. White and A. T. Nelson, *J. Nucl. Mater.*, 2017, **484**, 245-257.
7. X. Guo, J. T. White, A. T. Nelson, A. Migdisov, R. Roback and H. Xu, *J. Nucl. Mater.*, 2018, **507**, 44-49.
8. T. Le Bihan, H. Noël and P. Rogl, *J. Alloy. Compd.*, 1996, **240**, 128-133.
9. J. T. White, A. T. Nelson, D. D. Byler, J. A. Valdez and K. J. McClellan, *J. Nucl. Mater.*, 2014, **452**, 304-310.
10. S. C. Middleburgh, R. W. Grimes, E. J. Lahoda, C. R. Stanek and D. A. Andersson, *J. Nucl. Mater.*, 2016, **482**, 300-305.
11. R. C. Birtcher, J. W. Richardson and M. H. Mueller, *J. Nucl. Mater.*, 1996, **230**, 158-163.
12. M. R. Finlay, G. L. Hofman and J. L. Snelgrove, *J. Nucl. Mater.*, 2004, **325**, 118-128.
13. S. J. Zinkle, K. A. Terrani, J. C. Gehin, L. J. Ott and L. L. Snead, *J. Nucl. Mater.*, 2014, **448**, 374-379.
14. Y. B. Miao, J. Harp, K. Mo, S. Bhattacharya, P. Baldo and A. M. Yacout, *J. Nucl. Mater.*, 2017, **484**, 168-173.
15. A. Berche, C. Rado, O. Rapaud, C. Gueneau and J. Rogez, *J. Nucl. Mater.*, 2009, **389**, 101-107.
16. U. Carvajal-Nunez, T. A. Saleh, J. T. White, B. Maiorov and A. T. Nelson, *J. Nucl. Mater.*, 2018, **498**, 438-444.
17. U. Carvajal-Nunez, M. Elbakhshwan, N. Mara, J. White and A. Nelson, *JOM-US*, 2018, **70**, 203-208.
18. E. S. Wood, J. T. White and A. T. Nelson, *J. Nucl. Mater.*, 2017, **489**, 84-90.
19. K. Johnson, V. Strom, J. Wallenius and D. A. Lopes, *J Nucl Sci Technol*, 2017, **54**, 280-286.
20. E. Jossou, U. Eduok, N. Y. Dzade, B. Szpunar and J. A. Szpunar, *Phys. Chem. Chem. Phys.*, 2018, **20**, 4708-4720.
21. P. C. Burns, R. C. Ewing and A. Navrotsky, *Science*, 2012, **335**, 1184-1188.
22. P. Villars and L. Calvert, *American Society of Metals, Cleveland, OH*, 1991.
23. S. Yagoubi, S. Heathman, A. Svane, G. Vaitheeswaran, P. Heines, J.-C. Griveau, T. Le Bihan, M. Idiri, F. Wastin and R. Caciuffo, *J. Alloy. Compd.*, 2013, **546**, 63-71.
24. Y. Zhang and A. D. R. Andersson, *A thermal conductivity model for U-Si compounds*, Los Alamos National Laboratory, Los Alamos, 2017.
25. C.-K. Chung, X. Guo, G. Wang, J. T. White, A. T. Nelson, A. Shelyug, H. Boukhalfa, P. Yang, E. R. Batista, A. A. Migdissov, R. C. Roback, A. Navrotsky and H. Xu, *J. Alloy. Compd.*, 2019, ***submitted***.
26. C. B. Alcock and P. Grieveson, *J. I. Met.*, 1962, **90**, 304.

27. P. Gross, C. Hayman and H. Clayton, in *Thermodynamics of nuclear materials*, International Atomic Energy Agency, Vienna, 1962, pp. 653-665.
28. J. Zhang, A. Celestian, J. B. Parise, H. Xu and P. J. Heaney, *Am. Mineral.*, 2002, **87**, 566-571.
29. H. Xu, Y. Zhao, J. Zhang, D. D. Hickmott and L. L. Daemen, *Phys. Chem. Miner.*, 2007, **34**, 223-232.
30. H. Xu, J. Zhang, Y. Zhao, G. D. Guthrie, D. D. Hickmott and A. Navrotsky, *Am. Mineral.*, 2007, **92**, 166-173.
31. Y. Wang, J. Zhang, H. Xu, Z. Lin, L. L. Daemen, Y. Zhao and L. Wang, *Appl. Phys. Lett.*, 2009, **94**, 071904.
32. H. Xu, Y. Zhao, J. Zhang, Y. Wang, D. D. Hickmott, L. L. Daemen, M. A. Hartl and L. Wang, *Am. Mineral.*, 2010, **95**, 19-23.
33. J. Zhu, H. Xu, J. Zhang, C. Jin, L. Wang and Y. Zhao, *J. Appl. Phys.*, 2011, **110**, 084103.
34. Z. Quan, Z. Luo, Y. Wang, H. Xu, C. Wang, Z. Wang and J. Fang, *Nano Lett.*, 2013, **13**, 3729-3735.
35. S. Wang, X. Yu, J. Zhang, Y. Zhang, L. Wang, K. Leinenweber, H. Xu, D. Popov, C. Park and W. Yang, *J. Superhard Mater.*, 2014, **36**, 279-287.
36. J. Zhu, J. Zhang, H. Xu, S. C. Vogel, C. Jin, J. Frantti and Y. Zhao, *Sci. Rep.*, 2014, **4**, 3700.
37. A. Migliori and J. L. Sarrao, *Resonant ultrasound spectroscopy: applications to physics, materials measurements, and nondestructive evaluation*, Wiley New York, 1997.
38. X. Lü, Y. Wang, C. C. Stoumpos, Q. Hu, X. Guo, H. Chen, L. Yang, J. S. Smith, W. Yang and Y. Zhao, *Adv. Mater.*, 2016, **28**, 8663-8668.
39. G. Bounos, M. Karnachoriti, A. G. Kontos, C. C. Stoumpos, L. Tsetseris, A. Kaltzoglou, X. Guo, X. Lü, Y. S. Raptis and M. G. Kanatzidis, *J. Phys. Chem. C*, 2018, **122**, 24004-24013.
40. B. H. Toby and R. B. Von Dreele, *J. Appl. Cryst.*, 2013, **46**, 544-549.
41. P. Thompson, D. Cox and J. Hastings, *J. Appl. Cryst.*, 1987, **20**, 79-83.
42. H. W. Xu, M. E. Chavez, J. N. Mitchell, T. J. Garino, H. L. Schwarz, M. A. Rodriguez, D. X. Rademacher and T. M. Nenoff, *J. Am. Ceram. Soc.*, 2015, **98**, 2634-2640.
43. H. W. Xu, X. F. Guo and J. M. Bai, *Phys. Chem. Miner.*, 2017, **44**, 125-135.
44. W. Zachariasen, *Acta Crystallogr.*, 1949, **2**, 94-99.
45. R. U. Ichikawa, R. H. Garcia, A. S. d. Silva, X. Turrillas, A. M. Saliba-Silva, N. B. Lima and L. G. Martinez, Belo Horizonte, MG, Brazil, 2017.
46. R. W. Wyckoff, *Crystal structures. vol. 1*, Interscience Publ., 1971.
47. J. Gonzalez-Platas, M. Alvaro, F. Nestola and R. Angel, *J. Appl. Cryst.*, 2016, **49**, 1377-1382.
48. R. J. Angel, M. Alvaro and J. Gonzalez-Platas, *Z. Kristallogr. Cryst. Mater.*, 2014, **229**, 405-419.
49. D. L. Heinz and R. Jeanloz, *J. Appl. Phys.*, 1984, **55**, 885-893.
50. F. Birch, *Phys. Rev.*, 1947, **71**, 809.
51. S. Pugh, *Lond. Edinb. Dubl. Phil. Mag.*, 1954, **45**, 823-843.
52. A. Dwight, *Study of the uranium-aluminum-silicon system*, Argonne National Lab., IL (USA), 1982.
53. W. Köster and H. Franz, *Metall. Rev.*, 1961, **6**, 1-56.
54. J. Yang, J. Long, L. Yang and D. Li, *J. Nucl. Mater.*, 2013, **443**, 195-199.